ARTICLE   OPEN

Check for updates

Modeling the effects of salt concentration on aqueous and organic electrolytes

Stephanie C. C. van der Lubbe [1] and Pieremanuele Canepa [1,2,3 ✉]

Understanding the thermodynamic properties of electrolyte solutions is of vital importance for a myriad of physiological and technological applications. The mean activity coefficient $\gamma_\pm$ is associated with the deviation of an electrolyte solution from its ideal behavior and may be obtained by combining the Debye-Hückel (DH) and Born (B) equations. However, the DH and B equations depend on the concentration and temperature-dependent static permittivity of the solution $\varepsilon_r(c, T)$ and the size of the solvated ions r_i, whose experimental data is often not available. Here, we use a combination of molecular dynamics and density functional theory to predict $\varepsilon_r(c, T)$ and r_i, which enables us to apply the DH and B equations to any technologically relevant aqueous and nonaqueous electrolyte at any concentration and temperature of interest.

INTRODUCTION

The interplay between salt concentration and thermodynamic properties of electrolyte solutions is of vital importance for many physiological and technological applications, e.g. biochemistry, catalysis, energy storage, and materials science[1,2]. For example, the performance of energy storage devices, such as batteries and electrical double-layer capacitors depends entirely on the ionic conductivity, transference number, and electrochemical and thermal stability window of electrolytes. These electrolyte properties are determined by a complex interplay between the types of solvents, salts, and additives used, and are furthermore strongly dependent on the concentration and operating temperature of the environment[3–7]. Understanding the concentration and temperature dependence of the thermodynamic properties of an electrolyte for any given solvent/salt combination is therefore essential for selecting the proper electrolyte and further optimization of its properties.

In an electrolytic medium, the mean activity coefficient $\gamma_\pm$ relates to the change in chemical potential $\Delta\mu$ when going from an ideal system, in which all interactions (i.e. solvent-solvent, ion-solvent, ion-ion) are considered to be the same, to a real, nonideal system with component-specific intermolecular interactions[8,9]:

$$\Delta\mu = RT \ln \gamma_\pm \qquad (1)$$

where R is the gas constant and T is the temperature of the solution. Knowledge of $\gamma_\pm$ allows for the derivation of the thermodynamic factor $1 + d\ln(\gamma_\pm)/d\ln(c)$ (where c is the molar concentration), which is crucial for rationalizing and predicting the battery cell performance[10–13]. Additionally, $\gamma_\pm$ may be used to compute the freezing point depression when going from a pure solvent to the concentrated electrolyte[14]. Recently, the activity coefficient has been related to the upshift of the lithium metal anode potential[15]. Clearly, knowledge of activity coefficients of technologically relevant electrolytes is of primary importance, and many models have been developed to compute $\gamma_\pm$ as a function of electrolyte concentration and temperature for both weak and strong electrolytes[2,14,16–19].

One of the most widely used theories to calculate $\gamma_\pm$ is the Debye-Hückel (DH) model, which provides a mathematical framework to quantify ion-ion interactions in dilute electrolytes[2,20]. The DH model predicts an asymptotic decay of $\gamma_\pm$ as the salt concentration c increases[8,16,20]. However, for many electrolyte systems, the measured $\gamma_\pm$ values show inflection points after which $\gamma_\pm$ increase with higher c, often exceeding values of 1[10,11,21]. Therefore, the real behavior of electrolyte systems clearly deviates from the predicting capabilities of the DH model. This nonmonotonic behavior of real solutions has been associated with the ion-solvent interactions[16], and may be restored by including the Born (B) solvation term[22]. Combining the DH and Born (B) equations (thereafter abbreviated as DH+B) has been shown to improve the predictive power of the model for activity coefficients of aqueous electrolytes[17,23,24].

The main advantage of the DH+B model is that it is nearly parameter-free, except for the physically meaningful ionic radii and the static permittivity ε_r of the solution. This means that the DH+B model does not need to be fitted on experimental data, thereby circumventing the necessity for scarcely[18,25] available experimental activity coefficients. Furthermore, the mathematical simplicity of the DH+B model (see later Eqs. (2) and (4)) makes it straightforward to understand and implement its governing equations in the treatment of electrolyte solutions.

Within the DH+B framework, previous studies made use of experimental values of ε_r and the Born solvation radii R^B derived from experimental Gibbs solvation energies[16,24,26]. However, as ε_r and the Gibbs solvation energies (and thus R^B) are often not available, in this work we set a rigorous protocol for predicting ε_r and R^B from simulations, in particular, using molecular dynamics (MD) and density functional theory (DFT) calculations. This framework enables us to apply the DH+B model on any solvent/salt combination at any concentration and temperature of interest.

The aim of this work is twofold. Using our protocol, (i) we predict $\gamma_\pm$ for aqueous electrolytes and probe the performance of the DH+B model with computed values for ε_r and R^B. (ii) We then

---

[1]Department of Materials Science and Engineering, National University of Singapore, 9 Engineering Drive 1, 117575 Singapore, Singapore. [2]Department of Chemical and Biomolecular Engineering, National University of Singapore, 4 Engineering Drive 4, 117585 Singapore, Singapore. [3]Department of Electrical and Computer Engineering and Texas Center for Superconductivity, University of Houston, Houston, TX 77204, USA. ✉email: pcanepa@central.uh.edu
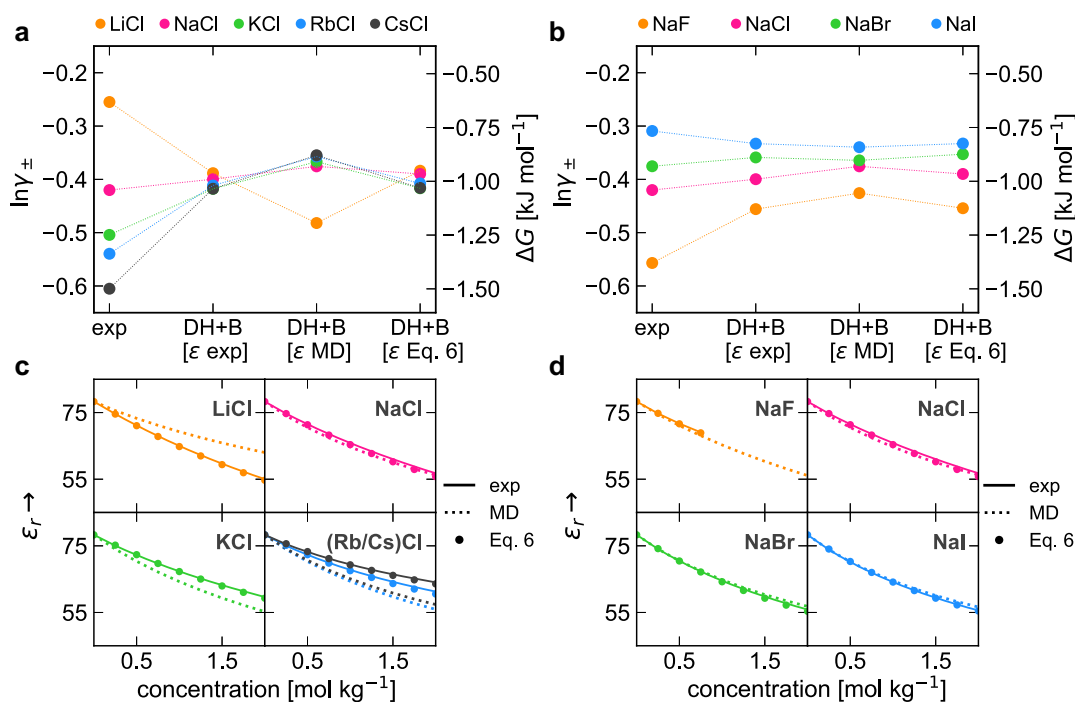
Fig. 1 Mean activity coefficients $\gamma_\pm$, Gibbs solvation energies and static permittivities ε_r of aqueous electrolytes. Panels (**a**, **b**) show the mean activity coefficient $\ln\gamma_\pm$ and ΔG in kJ mol^{-1} at 1 mol kg^{-1} for XCl (X = Li, Na, K, Rb, Cs) and NaX (X = F, Cl, Br, I) in aqueous solution at 298 K. Experimental data taken from ref. [21]. DH+B was computed by using ε_r from refs. [28,29], MD simulations or via Eq. (6). The ε_r^{exp} (solid line), ε_r^{MD} (dashed line) and $\varepsilon_r^{Eq.\,6}$ (dots) as a function of the concentration in mol kg^{-1} are shown in (**c**) for XCl and (**d**) for NaX. Dashed lines in (**a**, **b**) are shown for visual guidance.

apply the DH+B framework to nonaqueous organic electrolytes, which are highly relevant for commercial energy storage devices, including rechargeable batteries and supercapacitors. A useful guideline is provided to estimate the predictive accuracy of the DH+B model for technologically relevant electrolytes, for which the DH+B model may aid in understanding and predicting the thermodynamic properties.

RESULTS

Aqueous electrolytes

We begin by benchmarking the predictive capabilities of the DH+B model in reproducing reported experimental values of $\gamma_\pm$ of aqueous solutions with alkali metal chloride binary salts, with formula XCl (with X = Li, Na, K, Rb, and Cs) at 1 mol kg^{-1} (Fig. 1a). All DH+B data was generated with computed Born radii and with the solution static permittivity obtained from either available experimental data or MD simulations. In Fig. 1b the same approach is used for aqueous solutions of sodium halide salts, i.e. NaX (with X = F, Cl, Br, and I) at 1 mol kg^{-1}. This concentration was chosen because it is close to the salt concentration commonly used in battery electrolytes and supercapacitors[27]. Supplementary Figure 1 explores a wider concentration range from the infinitely dilute situation to a highly concentrated regimes (4 mol kg^{-1}).

The experimental $\gamma_\pm$ values become smaller for increasing cation sizes, following the order Li$^+$ > Na$^+$ > K$^+$ > Rb$^+$ > Cs$^+$ (Fig. 1a). A smaller value for $\gamma_\pm$ corresponds to a more negative Gibbs free energy ΔG (right y-axes of Fig. 1a, b, see also Eq. (1)). A decrease in $\gamma_\pm$ with increasing cation size has been associated with the smaller cation binding more tightly to the solvent ions, resulting in a larger decrease in the static permittivity (Supplementary Fig. 2), and hence a decrease in ion solubility.

The dataset obtained with the DH+B model using the available experimental[28,29] ε_r (i.e. ε_r^{exp}) results in all NaX electrolytes having a very similar values of $\gamma_\pm$. However, at ~1.5 mol kg^{-1}, the data

points separate from each other, reproducing the experimental trend over the remaining concentration range up to 4 mol kg^{-1} (Supplementary Fig. 1). Replacing the experimental for the computational static permittivity ε_r (i.e. ε_r^{MD}) in the DH+B model results in a poorer agreement between the predicted and experimental $\gamma_\pm$. Indeed, $\gamma_\pm^{DH+B}$ is almost identical for NaCl, KCl, RbCl and CsCl, but LiCl has the smallest, instead of the largest $\gamma_\pm$ in the XCl series.

These results can be understood by looking at the computed static permittivity (Fig. 1c). The MD simulations tend to overestimate ε_r for LiCl (i.e. ε_r^{MD} decreases too slowly), whereas the static permittivity of other alkali metal chlorides is underestimated (i.e. ε_r^{MD} decreases too rapidly). As a decrease in static permittivity results in an increase in $\gamma_\pm^B$, underestimating the decrease in ε_r translates into $\gamma_\pm^{DH+B}$ values that are too small for LiCl (see also Supplementary Fig. 3). Values of activity coefficients below 1 (i.e. a negative value for $\ln\gamma_\pm$) describe situations in which the ions prefer to be in the concentrated instead of infinitely dilute electrolyte, as is evident from the corresponding negative Gibbs free energy change. Hence, underestimating the activity coefficient for LiCl means that its preference to be in the concentrated electrolyte is overestimated.

When obtaining the static permittivity via Eq. (6), i.e. $\varepsilon_r^{Eq.\,6}$ (Fig. 1a), the NaX electrolytes recover a very similar value for $\gamma_\pm$ at 1 mol kg^{-1}. Around ~1.5 mol kg^{-1}, the data points separate from each other and correctly reproduce the experimental values for $\gamma_\pm$ over the remaining concentration range for each electrolyte (see Supplementary Fig. 1). As shown in Fig. 1c, the static permittivities obtained with Eq. 6 overlap almost perfectly with ε_r^{exp}, which explains why the activity coefficients obtained with $\varepsilon_r^{Eq.\,6}$ are as good as those obtained with ε_r^{exp}.

The DH+B model performs significantly better for the Na-halide series (Fig. 1b) compared to their Li-analogues. With NaF having the smallest and NaI having the largest values of $\gamma_\pm$, the experimental trend is correctly reproduced by the DH+B model

with ε_r^{exp}. Furthermore, the values of $\gamma_\pm^{exp}$ and $\gamma_\pm^{DH+B}$ are in good agreement for NaCl, NaBr, and NaI. For NaF, the DH+B model gives a higher activity coefficient than $\gamma_\pm^{exp}$, meaning that NaF preference to be in the concentrated electrolyte is underestimated by the DH+B model. Ion pairs of similar sizes, such as NaF, are less soluble than ion pairs of different sizes[30]. Furthermore, less soluble salts will show a less pronounced decrease in the static permittivity because fewer solvent molecules will participate in the solvation of the ions[31]. Should this be the case, we would expect lower predicted activity coefficients with the DH+B model. A possible explanation for the difference between $\gamma_\pm^{exp}$ and $\gamma_\pm^{DH+B}$ for NaF may be that the decrease in static permittivity of NaF is overestimated due to the highly localized charge on the bare fluoride ion, F^-.

When using static permittivities estimated from MD simulations ε_r^{MD}, the difference between computed values of $\gamma_\pm$ becomes smaller, but the relative order of the $\gamma_\pm$ values is still in agreement with the experimental trend. This improved performance (in comparison with the binary alkali metal chlorides) is mostly due to the computed values for ε_r^{MD}, which are much closer to their experimental values (Fig. 1d). When using $\varepsilon_r^{Eq. 6}$ in the DH+B equations, the difference between the values for $\gamma_\pm$ increases, approaching the values for $\gamma_\pm$ as obtained with ε_r^{exp}. Given the nearly perfect overlap between ε_r^{exp} and $\varepsilon_r^{Eq. 6}$ (see Fig. 1d), these results are in line with expectations.

Nonaqueous electrolytes

It is instructive to analyze the contribution of ε_r to the activity coefficient associated with the DH term ($\gamma_\pm^{DH}$) and the Born term ($\gamma_\pm^B$), as nonaqueous electrolytes often display a lower static permittivity than their aqueous counterparts. Figure 2 displays the values of $\gamma_\pm^{DH}$ and $\gamma_\pm^B$ as a function of the salt concentration and change in the solution static permittivity ε_r^{soln}, respectively. In Fig. 2, each color corresponds to a different static permittivity of the solvent ε_r^{solv}. On one hand, from Fig. 2a, $\gamma_\pm^{DH}$ becomes smaller with a lower static permittivity, and this decrease becomes more pronounced for smaller values of ε_r. On the other hand, for the Born term, (Fig. 2b), $\gamma_\pm^B$ increases exponentially with a decrease in ε_r^{soln}, and this increase in $\gamma_\pm^B$ becomes more pronounced for electrolytes with low solvent's static permittivity ε_r^{solv}. As a consequence, both $\gamma_\pm^{DH}$ and $\gamma_\pm^B$ become increasingly sensitive to the quality of the static permittivity of the solution with lower permittivity electrolytes.

We then move on to the application of the DH+B model to nonaqueous electrolytes, which are prevalent in Li and Na-ion batteries and supercapacitors. In Fig. 3, the activity coefficients $\gamma_\pm$ (left y-axes) and solution's static permittivity as computed with MD ε_r^{MD} (right y-axes) are plotted as a function of the salt concentration. Figure 3a charts the behavior of $LiClO_4$ (a common salt used in Li-ion batteries) in three different solvents, namely acetonitrile (ACN, $\varepsilon_r^{solv} = 36.0$ at 298 K), acetone (AC, $\varepsilon_r^{solv} = 21.0$ at 298 K), and dimethyl carbonate (DMC, $\varepsilon_r^{solv} = 3.1$ at 298 K). As shown in Fig. 3a, ACN displays the highest value of $\gamma_\pm^{exp}$, whereas DMC has the lowest $\gamma_\pm^{exp}$ over the whole range of concentration (solid lines). This trend is correctly reproduced by the DH+B model (dashed lines). Furthermore, $\gamma_\pm^{exp}$ and $\gamma_\pm^{DH+B}$ are in good agreement for the ACN and AC-based electrolytes. However, for DMC, the agreement between $\gamma_\pm^{exp}$ and $\gamma_\pm^{DH+B}$ appears extremely poor – this trend appears more evident when plotting the data in logarithmic scale (see Supplementary Fig. 5). For example, at 1 mol kg^{-1} $\gamma_\pm^{exp} = 0.002$, whereas $\gamma_\pm^{DH+B} = 3.61 \times 10^{-16}$, which equates to a difference in ΔG of 72.7 kJ mol^{-1}. This is a consequence of ε_r increasing (instead of decreasing) with higher salt concentrations, an effect that has been previously reported for low permittivity electrolytes[14,32,33]. As a result, both $\gamma_\pm^{DH} \ll 1$ and $\gamma_\pm^B \ll 1$ (Supplementary Fig. 5), resulting in extremely small total values of $\gamma_\pm^{DH+B}$.
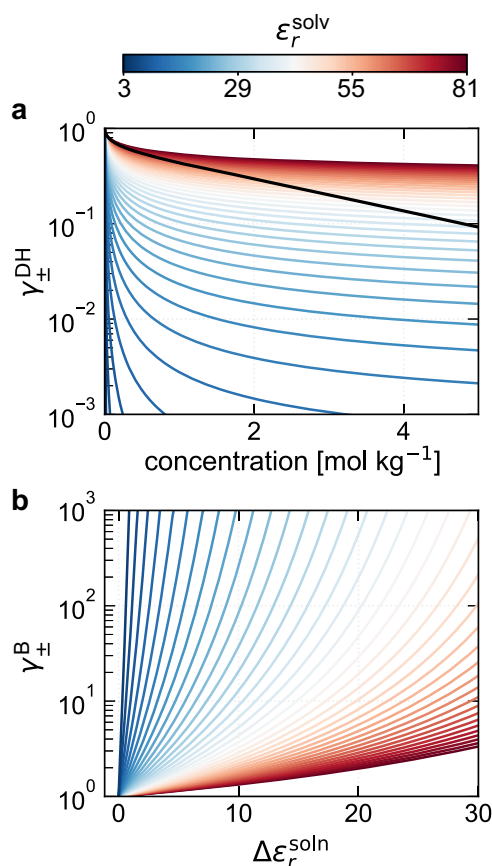
Fig. 2 The effect of the static permittivity on the Debye-Hückel and Born activity coefficients. Panel (**a**) shows $\gamma_\pm^{DH}$ as a function of the concentration for LiCl at 298 K. The data were generated by using a constant ε_r (instead of the concentration-dependent ε_r) in the Debye-Hückel equation with a step size of 2 in the ε_r range of 81 to 3. Each color corresponds to a different value for ε_r^{solv}, and the black line corresponds to $\gamma_\pm^{DH}$ when using the concentration-dependent ε_r for aqueous LiCl. In panel (**b**) the $\gamma_\pm^B$ is depicted as a function of the change in the solution static permittivity ε_r^{soln}. Different colors correspond to the static permittivity of the solvent ε_r^{solv} (i.e. at infinite dilution). The data were generated with a step size of 2 in the ε_r range of 81 to 3. Plots extending to larger values of $\gamma_\pm$ are given in Supplementary Fig. 4.

We then analyze the effect of changing the type of salt while keeping the solvent constant, starting from LiBr, LiCl, and LiNO$_3$ in dimethyl sulfoxide (DMSO, $\varepsilon_r^{solv} = 46.5$). From Fig. 3b, the experimental $\gamma_\pm$ (solid lines) is largest for LiBr and smallest for LiNO$_3$. The opposite trend is obtained with the DH+B model up to 1.5 mol kg^{-1} (dashed lines). These results can be understood from ε_r^{MD} used in the DH+B model. For LiNO$_3$, the decrease in ε_r is most pronounced, presumably due to the larger anion size, whereas the decrease in ε_r is least pronounced for LiBr (see dots in Fig. 3b). While this larger decrease in ε_r results in both a smaller $\gamma_\pm^{DH}$ and larger $\gamma_\pm^B$, the effect on $\gamma_\pm^B$ is more pronounced (Supplementary Fig. 5). Hence, the resulting trend in $\gamma_\pm^{DH+B}$ is completely determined by the Born term, which increases at a higher rate for the electrolyte subjected to a stronger decrease in ε_r.

In Fig. 3c, we applied the DH+B model to ACN solutions of LiBr, LiPF$_6$ and lithium bis(trifluoromethanesulfonyl)imide (LiTFSI), with the latter two being common salts in Li-ion batteries. The experimental $\gamma_\pm$ is highest for the salt with the largest anion (i.e. LiTFSI) and lowest for the salt with the smallest anion (LiBr) over the whole concentration range. This experimental trend is correctly reproduced by the DH+B model, and is dictated by
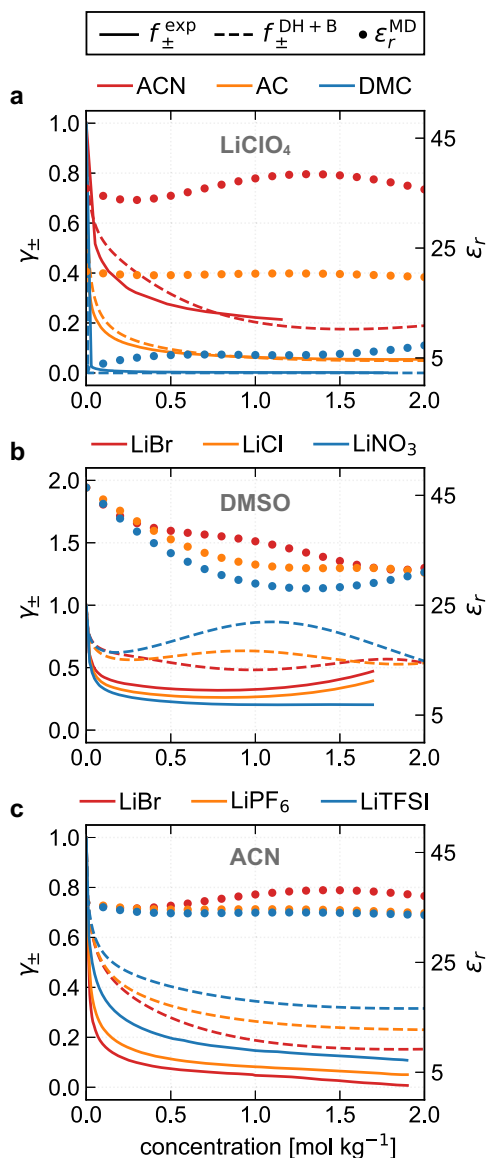
Fig. 3 Mean activity coefficients $\gamma_\pm$ and static permittivity ε_r^{MD} at 298 K as a function of the concentration in mol kg^{-1}. Panel (**a**) shows LiClO$_4$ in ACN, AC, and DMC. Panel (**b**) shows LiBr, LiCl, and LiNO$_3$ in DMSO. Panel (**c**) shows LiBr, LiPF$_6$, and LiTFSI in ACN. Experimental data obtained from ref. [43] are used in panel (**a**) and ref. [25] are used in (**b**, **c**). Solid lines: $\gamma_\pm^{exp}$. Dashed lines: $\gamma_\pm^{DH+B}$. Dots: ε_r^{MD}.

both the $\gamma_\pm^{DH}$ and $\gamma_\pm^{B}$ terms (Supplementary Fig. 5). The LiBr and LiPF$_6$ electrolytes share approximately the same values of $\gamma_\pm^{DH}$, whereas LiTFSI has much higher values for $\gamma_\pm^{DH}$ over the whole concentration range. At first glance, this trend of $\gamma_\pm^{DH}$ may appear surprising, as LiTFSI, together with LiPF$_6$, displays the lowest ε_r, whereas one should expect a general decrease of $\gamma_\pm^{DH}$ with lower values of ε_r (Fig. 2). The reason for this unexpected trend is that $\gamma_\pm^{DH}$ also decreases with a smaller ionic radius r_i. With Br$^-$ having the smallest (~1.95 Å) and TFSI$^-$ having the largest (~3.27 Å) radius among the salts considered here, the trend in $\gamma_\pm^{DH}$ is partly dictated by the ionic radius (Supplementary Fig. 6). Interestingly, variations in r_i on $\gamma_\pm^{DH}$ become more pronounced for electrolytes with a lower static permittivity (Supplementary Fig. 7). In practice, this signifies that $\gamma_\pm^{DH}$ becomes more sensitive to the choice of r_i for lower permittivity electrolytes. The ion-solvent term $\gamma_\pm^{B}$ is again
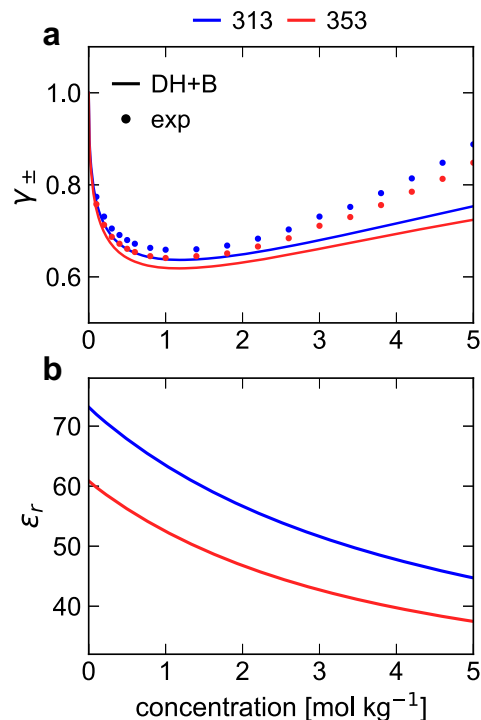
Fig. 4 Temperature dependence of the mean activity coefficient and static permittivity. Panel (**a**) shows the mean activity coefficients $\gamma_\pm$ for NaCl in H$_2$O as a function of the concentration in mol kg^{-1} at 313 K (blue) and 353 (red) K. Experimental data are obtained from ref. [34] and represented by dots. Solid lines represent the DH+B data. Panel (**b**) shows the static permittivity as a function of the concentration in mol kg^{-1} obtained with MD simulations.

dictated by the static permittivity, with a more pronounced decrease in ε_r leading to a larger increase in $\gamma_\pm^{B}$.

Temperature dependence

We assessed the performance of the DH+B model with computationally derived ε_r and R^B at higher temperatures T (313 and 353 K) for NaCl in H$_2$O. Figure 4 shows the activity coefficients and the static permittivities as a function of the salt concentration. In Fig. 4a, an increase in temperature results in a decrease of the experimental $\gamma_\pm$[34]; this trend has also been observed for other electrolytes[2,35,36]. The DH+B model with ε_r^{MD} reproduces this temperature dependence correctly. Furthermore, the computed values for $\gamma_\pm^{DH+B}$ are close to the experimental values of $\gamma_\pm$, and the monotonic behavior is correctly captured by the DH+B model for both temperatures.

In the case of LiCl in H$_2$O, we also computed the activity coefficients as a function of temperature. Despite the overestimation of experimental static permittivity by ε_r^{MD} (see Fig. 1c), the correct trend in $\gamma_\pm$ is again correctly recovered, see Supplementary Fig. 8.

DISCUSSION

In general, our analyses demonstrated that the DH+B model is highly sensitive to the quality of the electrolyte static permittivity ε_r, and this sensitivity increases with a lower value of ε_r. Therefore, an important point of consideration is the error in ε_r^{MD}, which directly influences the resulting predictions of $\gamma_\pm^{DH}$ and $\gamma_\pm^{B}$. The calculated values for ε_r^{MD} are subjected to systematic errors, arising, for example, from force fields (FFs) used for the organic electrolytes, which are not specifically designed to reproduce the static permittivity. We have partly accounted for these systematic
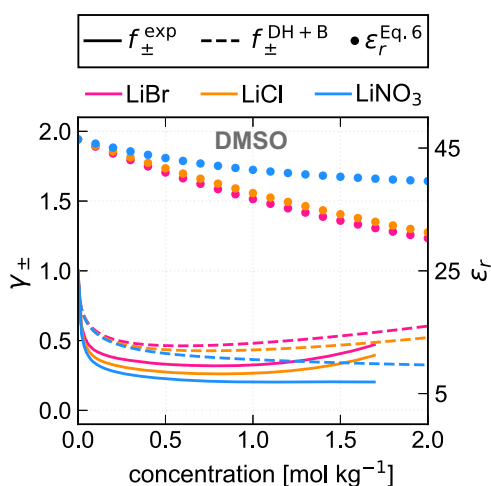
Fig. 5 Mean activity coefficients $\gamma_\pm$ and static permittivity $\varepsilon_r^{Eq.\,6}$ at 298 K as a function of the concentration in mol kg^{-1} for LiBr, LiCl, and LiNO$_3$ in DMSO. The parameters used in Eq. (6) are the same as those obtained for the corresponding salts in H$_2$O (see Supplementary Table 1). Experimental data obtained from ref. [25]. Solid lines: $\gamma_\pm^{exp}$. Dashed lines: $\gamma_\pm^{DH+B}$. Dots: $\varepsilon_r^{Eq.\,6}$.

errors by introducing *a posteriori* correction factors to the atomic charges. The atomic charges of the organic solvents were multiplied by a correction factor such that the experimental static permittivities of the pure solvent were correctly reproduced. The same correction factors were used for the solvent molecules in the concentrated electrolytes. The atomic charges of the salts were multiplied by a correction factor such that their dipole moment became equal to the dipole moment as obtained by DFT. These correction factors were only applied after completing the MD simulations and hence did not affect the molecular trajectories. More information is given in Supplementary Methods 3.

The accuracy of ε_r^{MD} may be further improved by parameterizing specific FFs on experimental values of ε_r of the pure solvents (whose data is widely available), in line with the approach adopted for the TIP4P/ε FF for water[37]. For the salts, the parameterization of FFs can be achieved at a single salt concentration. An optimized FF is then applied to any salt concentration of interest. We emphasize that this workflow substantially reduces the amount of experimental data necessary (to be used for the force field parameterization) in comparison with using the experimental values of ε_r directly in the DH+B equations.

An approach worth investigating is to parameterize the salt FFs on available experimental data for ε_r (e.g. aqueous electrolytes), and later use the same FFs when dissolving the salt in other solvent types. While the parameterization of dedicated FFs is beyond the scope of this study, a similar approach may be applied through Eq. (6). To demonstrate this concept, we utilized the values of β and λ (the parameters of Eq. (6)) optimized for aqueous electrolytes (see Supplementary Table 1) to calculate the static permittivities $\varepsilon_r^{Eq.\,6}$ of the nonaqueous electrolytes. Specifically, we calculated $\varepsilon_r^{Eq.\,6}$ for LiBr, LiCl, and LiNO$_3$ in DMSO, which are the same systems as studied in Fig. 3b and for which experimental values for ε_r are available in H$_2$O. The results are visualized in Fig. 5, with the activity coefficient $\gamma_\pm$ plotted on the left y-axis, and the static permittivity $\varepsilon_r^{Eq.\,6}$ plotted on the right y-axis as a function of the concentration in mol kg^{-1}. The y-axes in Figs. 5, 3b share the same scale to enable direct comparison between the two sets of data.

Using the static permittivity derived from Eq. (6), we predicted the correct trend in $f_\pm^{DH+B}$ (i.e. LiNO$_3$ < LiCl < LiBr) over the whole concentration range, as depicted in Fig. 5. Values of $\gamma_\pm^{DH+B}$ are in close agreement with the experimental values $\gamma_\pm^{exp}$. This is a

significant improvement in comparison with using static permittivities derived from MDs ε_r^{MD}, which gave an incorrect trend in the value of $\gamma_\pm^{DH+B}$ (Fig. 3b).

The lack of experimental data makes it difficult to quantify any remaining errors in ε_r^{MD} and $\varepsilon_r^{Eq.\,6}$. Furthermore, the kinetic depolarization effect in experimental measurements is complex to estimate, making a direct comparison between experimental and calculated values for ε_r challenging[2,38], see Supplementary Discussion 1. The observation that ε_r does not only decrease but at some points also increase with an increase in salt concentration has recently been discussed by Yao et al. for several nonaqueous electrolytes[31]. They show that an increase in ε_r with higher salt concentrations is caused by the dipole moment of the associated salt, which can be larger than the dipole moment of the solvent molecules. For the electrolytes studied in our work, we also find that the salts have larger dipole moments than the solvent molecules (see Supplementary Fig. 9), which may lead to an increase in ε_r with increasing salt concentrations. However, to the best of our knowledge, this nonmonotonic behavior in ε_r has yet to be confirmed by experimental studies.

It is insightful to look at the general effect of a given error in ε_r on the activity coefficients $\gamma_\pm^{DH}$ and $\gamma_\pm^B$. We emphasize that the remaining part of the discussion applies to the static permittivity in a general sense, regardless of the method by which its value is obtained. For the DH term, a lower static permittivity gives a lower $\gamma_\pm^{DH}$, and this lowering becomes more pronounced with a lower ε_r (Fig. 2). Therefore, a given error in ε_r will have more pronounced effects on electrolytes with low static permittivity. In specific solvents prevalent in battery applications, such as DMC, we demonstrated that even small (i.e. < 1) deviations in ε_r translate into errors in $\gamma_\pm^{DH}$ of multiple orders of magnitude (e.g. 4 orders of magnitude for 1 mol LiCl when ε_r changes from 4 to 3, see Fig. 2). The increased sensitivity of $\gamma_\pm^{DH}$ to the quality of ε_r is further demonstrated in Supplementary Fig. 10.

For the Born term, the quality of $\gamma_\pm^B$ is dictated by both the static permittivity of the solvent (ε_r^{solv}) and the change in ε_r upon the addition of the salt (ε_r^{soln}). The effect of a given error in ε_r on the value of $\gamma_\pm^B$ is visualized in Supplementary Fig. 11. In line with Fig. 2, the uncertainty in $\gamma_\pm^B$ increases with larger changes in ε_r, and this effect becomes more pronounced for electrolytes with lower permittivity solvents. For example, for 2 mol kg^{-1} LiClO$_4$ in AC, the static permittivity of the solution has a value of 19.7, which corresponds to a change in ε_r of only 1.0 from pure AC. Given an error of ± 3 in the static permittivity, the lower and upper bounds in $\gamma_\pm^B$ (i.e. the values for $\gamma_\pm^B$ generated with $\varepsilon_r - 3$ and $\varepsilon_r + 3$, respectively) are 0.7 and 10.3, which corresponds to an uncertainty in $\gamma_\pm^B$ of 9.6 (see Supplementary Fig. 11). These results underline the increased sensitivity of the Born term for the quality of the static permittivity for lower permittivity solvents.

The resulting inaccuracies on $\gamma_\pm^{DH}$ and $\gamma_\pm^B$ caused by the errors in ε_r will partly cancel each other out, as an increase in ε_r leads to a simultaneous decrease in $\gamma_\pm^{DH}$ and increase in $\gamma_\pm^B$. However, the extent to which $\gamma_\pm^{DH}$ and $\gamma_\pm^B$ cancel out is difficult to predict, as this depends not only on the value of ε_r but also on the change in ε_r with respect to the pure solvent. An additional factor that affects the performance of the DH+B model is that any change in the ionic parameters r_i and R_i^B has a more pronounced effect when ε_r is lower, which introduces an additional (potentially large) uncertainty in $\gamma_\pm^{DH}$ and $\gamma_\pm^B$. Overall, the increasingly large errors in $\gamma_\pm^{DH}$ and $\gamma_\pm^B$ introduced with lower static permittivities means that DH+B-type models are less robust for low-permittivity electrolytes. Usually, electrolytes in energy storage devices carry higher permittivity solvents (e.g. EC:DMC, EC:DME, EC:PC:DMC, where PC=propylene carbonate)[3–5,7] to adequately dissolve the salts.

Since the performance of the DH+B model does not only depend on ε_r but also on the extent of change in ε_r with increasing salt concentration, the overall accuracy of the DH+B model

appears strongly system-specific. Therefore, Fig. 2 provides a useful guideline to estimate the predictive accuracy of the DH+B model for technologically relevant electrolytes.

In summary, we have applied the extended Debye-Hückel model in combination with the Born equation (DH+B) on a series of aqueous and organic electrolytes, which are highly relevant for energy storage applications. The experimentally measurable variables that enter the DH+B equations, namely the Born solvation radius R^B and solution's static permittivity ε_r, were obtained via computer simulations. This workflow circumvents the need for experimental data, which are difficult to determine and not always available, thereby allowing the use of the DH+B model on any electrolyte at any concentration and temperature of interest.

The DH+B model with computationally obtained parameters performs mostly satisfactorily for aqueous electrolytes and becomes increasingly inaccurate for nonaqueous electrolytes bearing low static permittivities, such as DMC, DME, and DEC. The accuracy of the resulting activity coefficients $\gamma_\pm^{DH+B}$ is affected by both the static permittivity ε_r of the solvent as well as the change in ε_r at technologically relevant concentrations. Overall, the DH+B model may aid in understanding and predicting the properties of relevant aqueous and organic electrolytes, which remains an important task in paving both scientific and technological progress.

METHODS

The Extended Debye-Hückel model

We have used the extended Debye-Hückel (EDH) model for describing the chemical potential μ associated with the ion-ion interactions in solution. Via Eq. (1), the activity coefficient $\gamma_\pm^{DH}$ is given by

$$\ln \gamma_\pm^{DH} = \frac{-\zeta k}{\varepsilon_r k_B T}\left(\frac{1}{1+ka}\right) \text{ with } \zeta = \frac{z_i^2 e_0^2}{8\pi\varepsilon_0} \tag{2}$$

where z_i, e_0, ε_0 and k_B are the charge number, the elementary charge, the vacuum permittivity, and the Boltzmann constant, ε_r is the relative static permittivity, and a is the ionic size. k is the inverse of the Debye-Hückel length:

$$k = \sqrt{\frac{N_A e_0^2}{\varepsilon_0 \varepsilon_r k_B T}\sum_i c_i z_i^2} \tag{3}$$

where N_A is Avogadro's constant and c_i is the molar concentration. Here, the ionic size a is the distance of closest approach between two ions, which is approximated as the sum of ionic radii of the cation and anion (Supplementary Table 2). ε_r was set to the static permittivity of the solution, which depends on the salt concentration c and the temperature T. Recently, Sun et al. have shown that the performance of EDH is superior over the full DH equations in predicting the activity coefficients for 14 aqueous electrolytes[24].

The Born equation

The ion-solvent interactions were described using the Born equation, which gives the electrostatic energy change when moving a charged, spherical ion from a vacuum to a continuous dielectric medium. Moving from an infinitely dilute regime to a concentrated solution, the associated activity coefficient γ_i^B is:

$$\ln \gamma_i^B(c, T) = \frac{\zeta}{R_i^B(T)}\left(\frac{1}{\varepsilon_r^{soln}(c, T)} - \frac{1}{\varepsilon_r^{solv}(T)}\right) \tag{4}$$

where R_i^B is the Born radius, and ε_r^{soln} and ε_r^{solv} are the static permittivity of the solution and the solvent, respectively. DFT calculations were used to compute the Gibbs solvation energy, from which the Born radius R^B was obtained via the Born equation. A comparison between the calculated Born radii and Born radii derived from experimental Gibbs solvation energies is given in the Supplementary Discussion 2.

The Static permittivity

The static permittivity of the solution ε_r was predicted with MD simulations by computing the cumulative average of the dipole moment M[39], using Eq. (5):

$$\varepsilon_r = 1 + \frac{\langle M^2 \rangle - \langle M \rangle^2}{3\varepsilon_0 V k_B T} \tag{5}$$

where V is the volume of the simulation box. We have also implemented the following relationship between ε_r and salt concentration c developed in Ref. [40]:

$$\varepsilon_r(c) = \varepsilon_r^{solv} e^{-\beta\cdot\arctan(\lambda c)} \tag{6}$$

where β and λ were fitted on three experimental data points per electrolyte. Notably, Eq. (6) reliably predicts the correct asymptotic behavior of $\varepsilon_r(c)$ as the concentration of the solute is increased[40]. Full methodological details are given in Supplementary Methods 1–4.

DATA AVAILABILITY

All data are available upon reasonable request to the corresponding author.

CODE AVAILABILITY

All molecular simulations in this work were performed using the LAMMPS code (release 18 Feb 2020)[41]. All density functional theory calculations were performed using the Gaussian 16 software[42], which is a licensed software package.

REFERENCES

1. Kontogeorgis, G. M. & Folas, G. K. *Thermodynamic models for industrial applications: from classical and advanced mixing rules to association theories* (John Wiley & Sons Ltd, Chichester, U.K, 2010).
2. Kontogeorgis, G. M., Maribo-Mogensen, B. & Thomsen, K. The Debye-Hückel theory and its importance in modeling electrolyte solutions. *Fluid Phase Equilibria* **462**, 130–152 (2018).
3. Ponrouch, A., Marchante, E., Courty, M., Tarascon, J.-M. & Palacín, M. R. In search of an optimized electrolyte for Na-ion batteries. *Energy Environ. Sci.* **5**, 8572–8583 (2012).
4. Ponrouch, A. et al. Non-aqueous electrolytes for sodium-ion batteries. *J. Mater. Chem. A* **3**, 22–42 (2015).
5. Monti, D. et al. Towards standard electrolytes for sodium-ion batteries: physical properties, ion solvation and ion-pairing in alkyl carbonate solvents. *Phys. Chem. Chem. Phys.* **22**, 22768–22777 (2020).
6. Bevilacqua, S. C., Pham, K. H. & See, K. A. Effect of the electrolyte solvent on redox processes in Mg-S batteries. *Inorg. Chem.* **58**, 10472–10482 (2019).
7. Logan, E. & Dahn, J. Electrolyte design for fast-charging Li-Ion batteries. *Trends Chem.* **2**, 354–366 (2020).
8. Bockris, J. O. & Reddy, A. K. N. *Modern electrochemistry 1: Ionics* (Kluwer Academic/Plenum Publishers, New York, 1998), 2nd edn.
9. Costa Reis, M. Ion activity models: the Debye-Hückel equation and its extensions. *ChemTexts* **7**, 9 (2021).
10. Valøen, L. O. & Reimers, J. N. Transport properties of LiPF₆-based Li-Ion battery electrolytes. *J. Electrochem. Soc.* **152**, A882–A891 (2005).
11. Stewart, S. & Newman, J. Measuring the salt activity coefficient in lithium-battery electrolytes. *J. Electrochem. Soc.* **155**, A458–A463 (2008).
12. Landesfeind, J. et al. Comparison of ionic transport properties of non-aqueous lithium and sodium hexafluorophosphate electrolytes. *J. Electrochem. Soc.* **168**, 040538 (2021).
13. Xu, K. Navigating the minefield of battery literature. *Commun. Mater.* **3**, 31 (2022).
14. Self, J., Bergstrom, H. K., Fong, K. D., McCloskey, B. D. & Persson, K. A. A theoretical model for computing freezing point depression of lithium-ion battery electrolytes. *J. Electrochem. Soc.* **168**, 120532 (2021).

15. Yamada, A., Takenaka, N., Ko, S. & Kitada, A. Liquid madelung potential as a descriptor for lithium metal electrodes. PREPRINT (Version 1) available at Research Square [https://doi.org/10.21203/rs.3.rs-1830373/v1] (2022).

16. Vincze, J., Valiskó, M. & Boda, D. The nonmonotonic concentration dependence of the mean activity coefficient of electrolytes is a result of a balance between solvation and ion-ion correlations. J. Chem. Phys. **133**, 154507 (2010).

17. Shilov, I. Y. & Lyashchenko, A. K. The role of concentration dependent static permittivity of electrolyte solutions in the Debye–Hückel theory. J. Phys. Chem. B **119**, 10087–10095 (2015).

18. Crothers, A. R., Radke, C. J. & Prausnitz, J. M. 110th Anniversary : Theory of activity coefficients for lithium salts in aqueous and nonaqueous solvents and in solvent mixtures. Ind. Eng. Chem. Res. **58**, 18367–18377 (2019).

19. Vrbka, L. et al. Ion-specific thermodynamics of multicomponent electrolytes: A hybrid HNC/MD approach. J. Chem. Phys. **131**, 154109 (2009).

20. Debye, P. & Hückel, E. The theory of electrolytes. I. Freezing point depression and related phenomena [Zur Theorie der Elektrolyte. I. Gefrierpunktserniedrigung und verwandte Erscheinungen]. Phys. Z. **24**, 185–206 (1923). Translated and typeset by Michael J. Braus (2020).

21. Hamer, W. J. & Wu, Y.-C. Osmotic coefficients and mean activity coefficients of uni-univalent electrolytes in water at 25℃. J. Phys. Chem. Ref. Data **1**, 1047–1099 (1972).

22. Born, M. Volumen und Hydratationswärme der Ionen. Z. Phys. **1**, 45–48 (1920).

23. Valiskó, M. & Boda, D. Comment on "The Role of Concentration Dependent Static Permittivity of Electrolyte Solutions in the Debye–Hückel Theory". J. Phys. Chem. B **119**, 14332–14336 (2015).

24. Sun, L., Lei, Q., Peng, B., Kontogeorgis, G. M. & Liang, X. An analysis of the parameters in the Debye-Hückel theory. Fluid Ph. Equilibria **556**, 113398 (2022).

25. Xin, N., Sun, Y., Radke, C. J. & Prausnitz, J. M. Osmotic and activity coefficients for five lithium salts in three non–aqueous solvents. J. Chem. Thermodynamics **132**, 83–92 (2019).

26. Shilov, I. Y. & Lyashchenko, A. K. Modeling activity coefficients in alkali iodide aqueous solutions using the extended Debye-Hückel theory. J. Mol. Liq. **240**, 172–178 (2017).

27. Giffin, G. A. The role of concentration in electrolyte solutions for non-aqueous lithium-based batteries. Nat. Commun. **13**, 5250 (2022).

28. Fawcett, W. R. & Tikanen, A. C. Role of solvent permittivity in estimation of electrolyte activity coefficients on the basis of the mean spherical approximation. J. Phys. Chem. **100**, 4251–4255 (1996).

29. Tikanen, A. C. & Fawcett, W. R. Application of the mean spherical approximation and ion association to describe the activity coefficients of aqueous 1:1 electro-lytes. J. Electroanal. Chem. **439**, 107–113 (1997).

30. Okamoto, R., Koga, K. & Onuki, A. Theory of electrolytes including steric, attrac-tive, and hydration interactions. J. Chem. Phys. **153**, 074503 (2020).

31. Yao, N. et al. An atomic insight into the chemical origin and variation of the dielectric constant in liquid electrolytes. Angew. Chem. Int. Ed. **60**, 21473–21478 (2021).

32. Self, J., Wood, B. M., Rajput, N. N. & Persson, K. A. The interplay between salt association and the dielectric properties of low permittivity electrolytes: The case of $LiPF_6$ and $LiAsF_6$ in dimethyl carbonate. J. Phys. Chem. C **122**, 1990–1994 (2018).

33. Lee, H. et al. Why does dimethyl carbonate dissociate Li salt better than other linear carbonates? critical role of polar conformers. J. Phys. Chem. Lett. **11**, 10382–10387 (2020).

34. Ensor, D. D. & Anderson, H. L. Heats of dilution of NaCl: Temperature dependence. J. Chem. Eng. Data **18**, 205–212 (1973).

35. Campbell, A. N. & Bhatnagar, O. N. Osmotic and activity coefficients of lithium chloride in water from 50 to 150 ℃. Can. J. Chem. **57**, 2542–2545 (1979).

36. Valiskó, M. & Boda, D. The effect of concentration- and temperature-dependent dielectric constant on the activity coefficient of NaCl electrolyte solutions. J. Chem. Phys. **140**, 234508 (2014).

37. Fuentes-Azcatl, R. & Alejandre, J. non-polarizable force field of water based on the dielectric constant: TIP4P/ε. J. Phys. Chem. B **118**, 1263–1272 (2014).

38. Hubbard, J. B., Colonomos, P. & Wolynes, P. G. Molecular theory of solvated ion dynamics. III. The kinetic dielectric decrement. J. Chem. Phys. **71**, 2652–2661 (1979).

39. de Leeuw, S. W., Perram, J. W. & Smith, E. R. Simulation of electrostatic systems in periodic boundary conditions. I. Lattice sums and dielectric constants. Proc. R. Soc. Lond. A **373**, 27–56 (1980).

40. Gao, H., Chang, Y. & Xiao, C. An analytical expression for dielectric decrement law. AIP Adv. **10**, 045109 (2020).

41. Thompson, A. P. et al. LAMMPS—a flexible simulation tool for particle-based materials modeling at the atomic, meso, and continuum scales. Comput. Phys. Commun. **271**, 108171 (2022).

42. Frisch, M. J. et al. Gaussian 16, Revision A.03 (2016).

43. Barthel, J., Neueder, R., Poepke, H. & Wittmann, H. Osmotic coefficients and activity coefficients of nonaqueous electrolyte solutions. part 2. lithium per-chlorate in the aprotic solvents acetone, acetonitrile, dimethoxyethane, and dimethylcarbonate. J. Solution Chem. **28**, 489–503 (1999).

AUTHOR CONTRIBUTIONS
The study was designed by both authors (S.C.C.L. and P.C.). The computational data were generated and analyzed by S.C.C.L. The initial draft of the paper was prepared by S.C.C.L. and was further edited by both authors. P.C. supervised all aspects of the work including the procurement of funding. Both authors approve of the final version of the paper and are accountable for all aspects of the work.

COMPETING INTERESTS
The authors declare no competing interests.

ADDITIONAL INFORMATION
Supplementary information The online version contains supplementary material available at https://doi.org/10.1038/s41524-023-01126-0.

Correspondence and requests for materials should be addressed to Pieremanuele Canepa.

Reprints and permission information is available at http://www.nature.com/reprints

Publisher's note Springer Nature remains neutral with regard to jurisdictional claims in published maps and institutional affiliations.